Supplemental Material

Tissue flows are tuned by actomyosin-dependent mechanics in developing embryos

R. Marisol Herrera-Perez, Christian Cupo, Cole Allan, Alicia B. Dagle, Karen E. Kasza

Department of Mechanical Engineering, Columbia University, New York, New York, 10027, USA Corresponding author: Karen E. Kasza, karen.kasza@columbia.edu

Supplemental movie captions

Movie S1. Cell shapes and tissue flow during germband extension in a control embryo. Cell outlines visualized with CIBN-pmGFP. Maximum intensity projection. Anterior left, ventral down.

Movie S2. Cell shapes and tissue flow during germband extension in an optoGEF embryo under continuous optogenetic activation. Cell outlines visualized with CIBN-pmGFP. Maximum intensity projection. Anterior left, ventral down.

Movie S3. Cell shapes and tissue flow during germband extension in an optoGAP embryo under continuous optogenetic activation. Cell outlines visualized with CIBN-pmGFP. Maximum intensity projection. Anterior left, ventral down.

Movie S4. Myosin II localization during germband extension in photoactivated control, optoGEF, and optoGAP embryos. Myosin II is visualized using an mCherry-tagged myosin regulatory light chain (magenta) and cell outlines are visualized with CIBN-pmGFP (green). Anterior left, ventral down. Each panel corresponds to a 30 x 30 μm region.

Supplemental figures

Figure S1

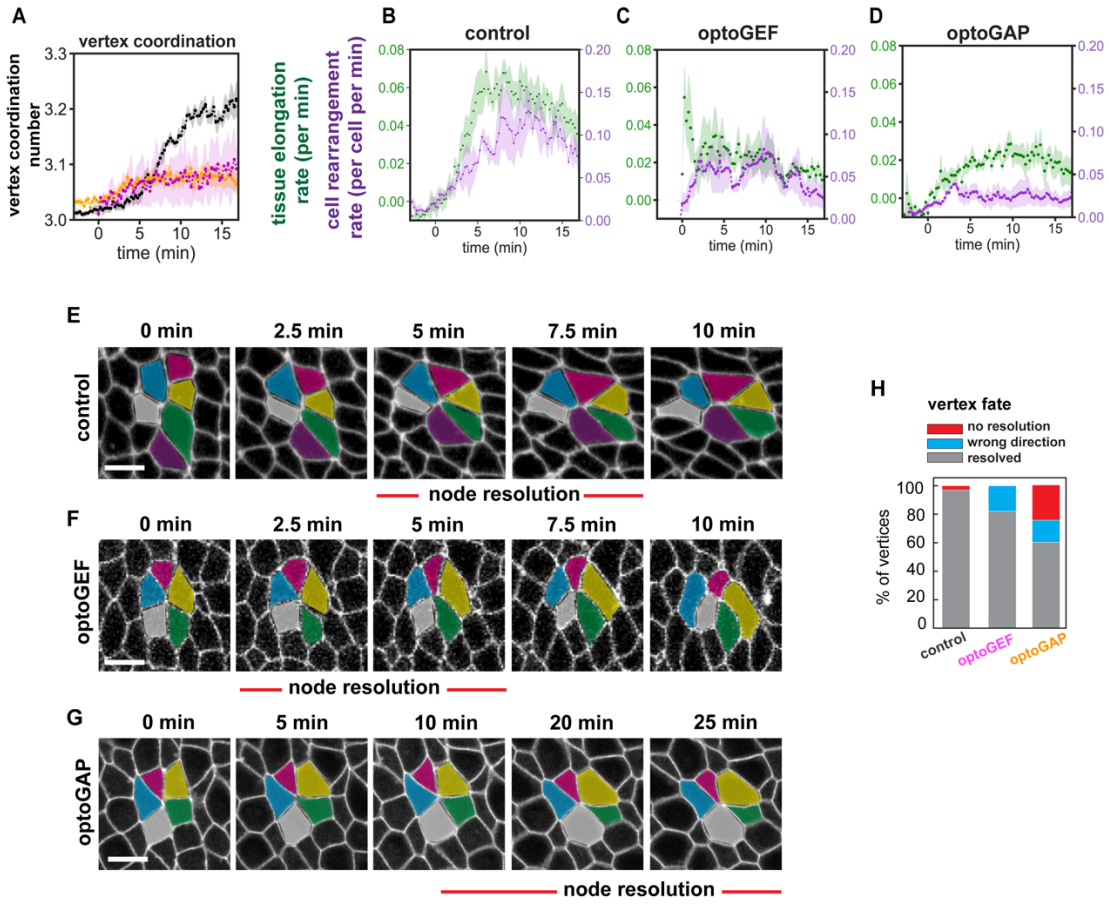

Figure S1. (A) Cell vertex coordination number represents the average number of cells meeting at a common vertex in the tissue. **(B-D)** Instantaneous rates of tissue elongation and cell rearrangements over time for control (B), optoGEF (C), and optoGAP (D) embryos. The mean ± SEM between embryos is shown, n=3-5 embryos per genotype. **(E-G)** Still images from time-lapse movies showing the progression of a cell rearrangement over time. optoGEF embryos showed increased numbers of newly formed edges oriented diagonally (not parallel) to the AP axis compared to controls. optoGAP embryos showed increased times to resolve a vertex during cell rearrangement compared to control or optoGEF embryos. Bars, 5 μm. **(H)** The fate of vertices formed through contraction of AP cell edges. The optoGAP and optoGEF embryos showed an increased percentage of vertices that did not resolve or aberrantly resolved to form an AP edge.

Figure S2

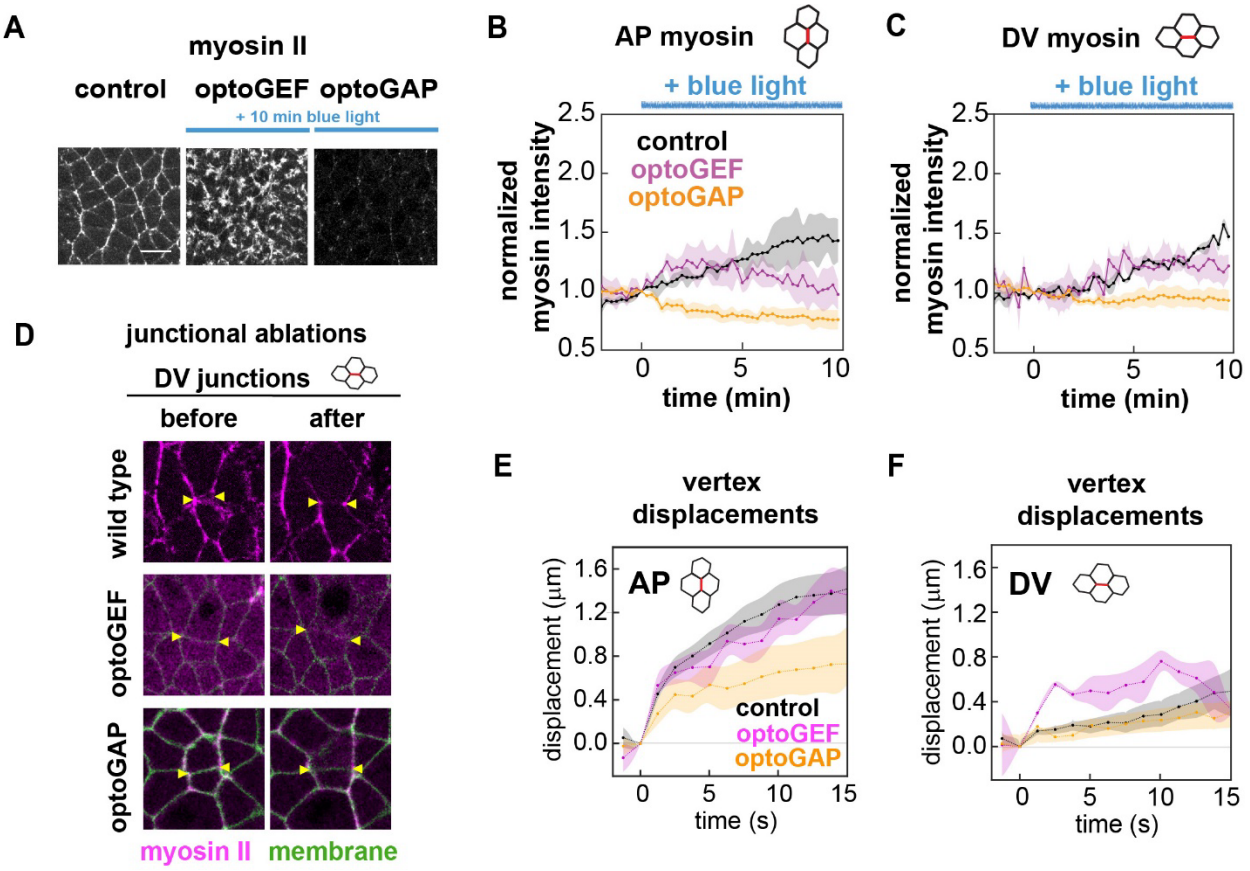

Figure S2. (A) Stills from movies of epithelial germband cells during *Drosophila* body axis elongation showing myosin II localization in control, optoGEF, and optoGAP embryos after continuous activation of the tool for 10 min. Bar, 10 μm. Maximum intensity projection of z-slices in the most apical 5 μm. Myosin II (myosin) was visualized using an mCherry-tagged myosin regulatory light chain (*sqh*) transgene. **(B-C)** Myosin II localization patterns in optogenetically manipulated germband tissue during *Drosophila* body axis elongation in control, optoGEF, and optoGAP embryos. Mean junctional myosin intensity before and during tool activation beginning at $t = 0$ (duration of blue light exposure indicated by blue line) at AP and DV junctions. Both optoGEF and optoGAP embryos exhibit decreased junctional myosin accumulation compared to controls, n=3-4 embryos, > 30 junctions/embryo **(D)** Ablations at DV cell junctions in optogenetically manipulated germband tissue. Cells before (left) and 1 min after (right) ablation. Myosin II (magenta), CIBN-pmGFP (green). Arrowheads indicate the vertices connected to the junction in which the cut was made. Anterior, left. Ventral, down. Image size, 20 x 20 μm. **(E-F)** Vertex displacements following ablations at AP or DV junctions. Mean ± SEM between junctions is shown, n=10-15 AP, 3-10 DV junctions per condition.

Figure S3

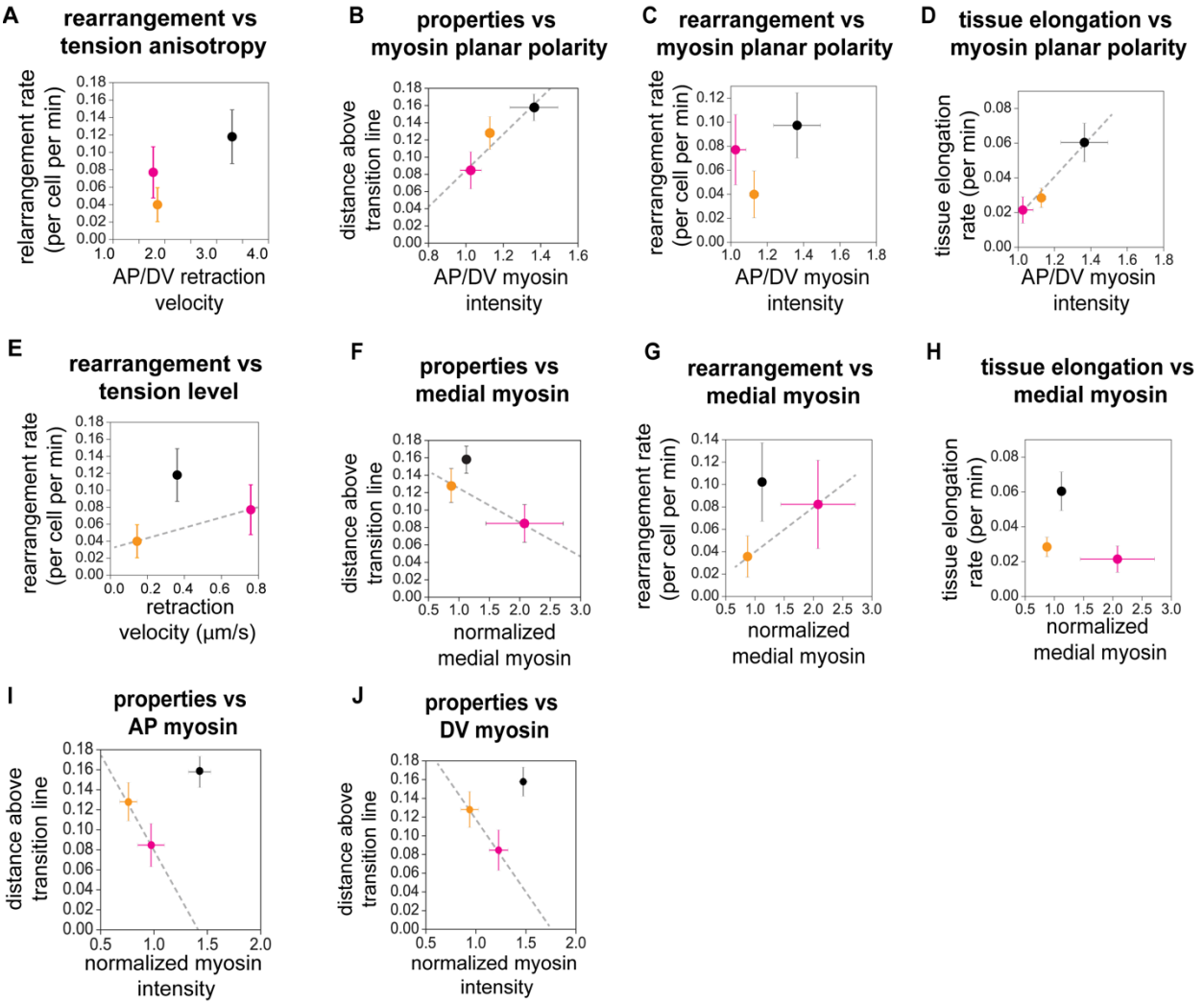

Figure S3. Relationships between tissue mechanical behaviors, tensions, and myosin localization patterns during convergent extension in photoactivated control, optoGEF, and optoGAP embryos: **(A)** Cell rearrangement rate vs tension anisotropy. As a readout of anisotropy, the ratio of AP to DV peak retraction velocities after ablation of junctional myosin was used, **(B)** predicted fluid-solid tissue properties vs. myosin planar polarity, **(C)** cell rearrangement rate vs. myosin planar polarity, **(D)** tissue elongation rate vs. myosin planar polarity, **(E)** cell rearrangement rate vs average magnitude of tissue retraction velocity after medial ablation, **(F)** predicted fluid-solid tissue properties vs. myosin intensity in the medial-apical domain, **(G)** cell rearrangement rate vs. myosin intensity in the medial-apical domain, **(H)** tissue elongation rate vs. myosin intensity in the medial-apical domain, **(I)** predicted fluid-solid tissue properties vs. myosin intensity at AP junctions, **(J)** predicted fluid-solid tissue properties vs. myosin intensity at DV junctions, Dashed lines, guides to the eye.